

NATIONAL ACADEMY OF SCIENCES OF UKRAINE

# SPACE RESEARCH IN UKRAINE

2018—2020

**Report  
to COSPAR**

*The Report Prepared by the Space Research Institute  
of NAS of Ukraine and SSA of Ukraine*

*Scientific Editor O. FEDOROV*

SRI NASU-SSAU  
Space Research Institute  
of National Academy of Sciences of Ukraine  
and State Space Agency of Ukraine  
Ukraine  
03680, Kyiv 187  
40, Glushkov Ave., building 4/1  
<http://www.ikd.kiev.ua>

NASU  
National Academy of Sciences of Ukraine  
Ukraine  
01601, Kyiv 30  
54, Volodymyrska St.  
<http://www.nas.gov.ua>

*The publication was funded within the framework of the Targeted Complex Program of the NAS of Ukraine  
«Scientific Bases of Functioning and Providing for Conditions for the Development  
of the Scientific and Publishing Complex of the NAS of Ukraine»*

*The edition is funded within the framework of the Nationwide Target Research  
and Engineering Space Program of Ukraine*

**Space research in Ukraine. 2018–2020** / Ed. O. Fedorov. — Kyiv:  
S78 Akadempriodyka, 2021. — 142 p.

ISBN 978-966-360-425-1

Report to COSPAR summarizes the results of space research performed during the years 2018–2020. This edition presents the current state of Ukrainian space science in the following areas: Space Astronomy and Astrophysics, Earth observation and Near-Earth Space Research, Life Sciences, Space Technologies and Materials Sciences. A number of papers are dedicated to the creation of scientific instruments for perspective space missions. Considerable attention paid to applied research of space monitoring of the Earth. The collection can be useful for a wide range of readers, interested in space research.

UDK 001.891(15)"2018/2020"

# CONTENTS

FOREWORD .....	4
<b>Space Astronomy and Astrophysics</b>	
GROUND-BASED SUPPORT OF SPACE MISSIONS BY UKRAINIAN RADIO TELESCOPES (A. Konovalenko, N. Kalinichenko, V. Zakharenko, O. Ulyanov, V. Dorovskyy, V. Melnik, A. Stanislavsky, P. Zarka, B. Cecconi, H. Rucker, V. Krupar, I. Bubnov, S. Yerin, P. Tokarsky, M. Sidorchuk, S. Stepin, L. Lytvinenko, Ya. Yatskiv, Yu. Shkuratov, N. Kuhai, N. Shevchuk, A. Brazhenko, V. Koshovyy, O. Ivantyshin, O. Lytvinenko, A. Romanchuk, A. Shevtsova, I. Kravtsov, V. Kharlanova) .....	5
<b>Near Earth Space Research</b>	
ATMOSPHERIC GRAVITY WAVES — THE MOST PROBABLE MECHANISM OF SEISMIC-IONOSPHERIC COUPLING (G. Lizunov, V. Korepanov, V. Pronenko, O. Piankova) .....	15
MODELLING THE INTERACTION OF SPACECRAFT WITH PLASMA FLOW, ELECTROMAGNETIC RADIATION, ELECTRIC AND MAGNETIC FIELDS IN THE EARTH'S IONOSPHERE (V. Shuvalov, Yu. Kuchugurnyi, D. Lazuchenkov) .....	29
CONCEPT OF THE PARTICLE MICROBURSTS SATELLITE EXPERIMENT WITH THE MiRA <sub>ep</sub> COMPACT INSTRUMENT ON THE 2U CUBESAT PLATFORM (O. Dudnik, V. Boiko, O. Yakovlev, V. Adamenko, R. Antypenko, A. Movchaniuk, N. Yezerkyi, A. Didenko, I. Lazariev, T. Gorbachova) .....	32
A PROTOTYPE OPERATIONAL SERVICE FOR LOCAL GEOMAGNETIC FORECAST (A. Parnowski, D. Vlasov) .....	40
RESULTS OF EXPERIMENTAL AND THEORETICAL STUDIES OF PHYSICAL PROCESSES IN THE IONOSPHERE OVER UKRAINE IN 2018–2020 (I. Dominin, L. Emelyanov, D. Kotov, S. Panasenko, L. Chernogor, M. Lyashenko, O. Bogomaz) .....	43
INFRASONIC, ATMOSPHERIC, AND IONOSPHERIC EFFECTS OF NATURAL AND MAN-MADE ORIGIN (L. Chernogor, V. Koshovyy, O. Ivantyshyn, B. Rusyn) ..	51
PHYSICAL EFFECTS IN THE ATMOSPHERE AND GEOSPACE ENVIRONMENT UNDER QUIET AND DISTURBED CONDITIONS (L. Chernogor, V. Rozumenko) .....	61
<b>Space Biology</b>	
SPACE BIOLOGY: RESULTS AND PROSPECTS (E. Kordyum, T. Borisova, N. Krisanova, N. Pozdnyakova, G. Shevchenko, L. Kozeko, S. Romanchuk, O. Lobachevska, Ya. Charkavtsiv, N. Kyiak, N. Zaimenko, B. Ivanytska, V. Brykov, L. Mischenko) .....	71
DEVELOPMENT OF AUTOPHAGY IN PLANT CELLS UNDER MICROGRAVITY: THE ROLE OF MICROTUBULES AND ATG8 PROTEINS IN AUTOPHAGOSOME FORMATION (A. Yemets, R. Shadrina, I. Horyunova, S. Plokhovska, O. Kravets, Y. Blume) .....	79
<b>Earth Observation from Space</b>	
ASSESSMENT OF SUSTAINABLE DEVELOPMENT GOALS WITHIN THE EUROPEAN NETWORK FOR OBSERVING OUR CHANGING PLANET (ERA-PLANET) (N. Kussul, A. Shelestov, M. Lavreniuk, B. Yailymov, O. Fedorov, L. Shumilo, H. Yailymova, S. Skakun, Y. Bilokonska, L. Kolos) .....	85
SDG INDICATOR 11.3.1 WITHIN HORIZON-2020 SMURBS (N. Kussul, A. Shelestov, L. Shumilo, M. Lavreniuk, B. Yailymov, H. Yailymova, S. Skakun, Y. Bilokonska) .....	91
AUTOMATION IN REMOTE SENSING DATA PRE-PROCESSING (V. Lukin, M. Uss, S. Abramov, I. Vasilyeva, G. Proskura, O. Ieremeiev, V. Abramova, O. Rubel, N. Kozhemiakina, V. Naumenko) .....	96
APPLICATION OF SPACE ENVIRONMENTAL MONITORING TO IDENTIFY DESERT LOCATIONS IN UKRAINE (V. Lyalko, L. Elistratova, A. Apostolov, I. Romanciuc) .....	104
ANTI-PANDEMIC MEASURES HELP TO REDUCE THE IMPACT OF THE GREENHOUSE EFFECT ON CLIMATE (V. Lyalko, A. Apostolov, E. Dorofey) .....	107
MONITORING OF SOLID DOMESTIC AND INDUSTRIAL WASTE LANDFILLS BY SPACE SURVEY MATERIALS IN THE LONG-WAVE IR RANGE (ON EXAMPLE OF GRIBOVICHY LANDFILL AND SPOIL TIP OF CHERVONOGRAD COAL PREPARATION PLANT) (V. Filipovych, A. Mychak, R. Shevchuk) .....	109
<b>Space Technologies and Materials Sciences</b>	
RESULTS OF DEVELOPMENT, MODELING, TESTING AND OPERATION OF THE POLYTAN SERIES NANOSATELLITES (B. Rassamakin, M. Ducheiko, N. Bayskov, S. Ostapchuk, A. Lauch, E. Lanevsky V. Hominich, A. Padun) .....	115
ROCKET SOUNDING SYSTEM FOR LOWER IONOSPHERE RESEARCH (S. Larkov, V. Prisiagnii, G. Lizunov, K. Volokh, S. Moskalenko, O. Piskun, O. Piankova, S. Pipko) .....	124
COMPUTER VISION SYSTEM FOR SPACECRAFT RELATIVE POSE DETERMINATION DURING RENDEZVOUS AND DOCKING (V. Gubarev, V. Vasylyev, V. Volosov, L. Maksymyuk, S. Melnychuk, N. Salnikov, V. Shevchenko, L. Godunok, S. Derkach) .....	127
DESIGN FEATURES OF THE STEP-F PARTICLE DETECTOR AND THE SPHINX SOLAR X-RAY SPECTROPHOTOMETER AS SEEDS FOR REVEALING SOME PECULIAR PROPERTIES OF THE EARTH RADIATION BELTS (O. Dudnik, J. Sylwester, M. Kowalski, P. Podgórski, H. Didenko, I. Zajitsevskiy, O. Perevertaylo) .....	133

---

## FOREWORD

The publication represents the results of space research and developments, performed by leading Ukrainian scientific teams in the years 2018–2020. Unfortunately, during this period, Ukrainian scientists were not supported by the National Space Programme, which was not developed and adopted by the Parliament. Therefore, this edition includes the works supported by the National Academy of Sciences and international grants in the following areas: Space Astronomy and Astrophysics, Near Earth Space Research, Space Biology, Earth Observation from Space, Space Technologies and Materials Science (according to the classification of COSPAR).

Section "Space Astronomy and Astrophysics" represents the review of the Institute of Radio Astronomy on synchronous coordinated ground-based support of space missions using Ukrainian radio telescopes UTR-2.

The second section includes the results of studying the processes in the Earth's atmosphere — ionosphere — magnetosphere system. The articles of Space Research Institute specialists are devoted to the mechanisms of seismic-ionospheric coupling and creation of operational service for local geomagnetic forecast. Researchers of the Institute of Technical Mechanics present the modeling of complicated interactions of a spacecraft with Earth ionosphere. The new concept of the particle microbursts satellite experiment advanced by the team of scientists including experts of the Institute of Radio Astronomy. Three articles reviews the different aspects of the interactions of Geospace environment with natural and man-made objects.

The next series of review articles represents the Ukrainian science centers activity in the Space Biology, Space Observation of the Earth and Space Technologies. Most of them dedicated to perspective space missions and utilization of space data for assessment the sustainable development goals.

In general, the presented review illustrates the current state and multidimensionality of the subjects of Ukrainian space science. Some of the results were obtained in the framework of international projects, programs and grants, including the European program Horizon 2020, and most of the results had been reported at the annual Ukrainian Conference on Space Research, international seminars and conferences.

The collection is intended for space scientists, post-graduate students and readers interested in space research.

---

# DESIGN FEATURES OF THE STEP-F PARTICLE DETECTOR AND THE SPHINX SOLAR X-RAY SPECTROPHOTOMETER AS SEEDS FOR REVEALING SOME PECULIAR PROPERTIES OF THE EARTH RADIATION BELTS

O. Dudnik<sup>1</sup>, J. Sylwester<sup>2</sup>, M. Kowaliński<sup>2</sup>, P. Podgórski<sup>2</sup>,  
H. Didenko<sup>3</sup>, I. Zajtsevskiy<sup>4</sup>, O. Perevertaylo<sup>5</sup>

<sup>1</sup> Institute of Radio Astronomy of NAS of Ukraine

<sup>2</sup> Space Research Centre of Polish Academy of Sciences

<sup>3</sup> Institute for Scintillation Materials of NAS of Ukraine

<sup>4</sup> Institute for Safety Problems of Nuclear Power Plants of NAS of Ukraine

<sup>5</sup> Scientific Production Company "Alex Detector" Limited Liability Company

---

The radiation belts of the Earth and the variations of high energy electron and proton fluxes in the magnetosphere are the targets for intensive exploration by the scientific community. Quickly grown number of artificial Earth satellites around the Earth supports the continuous improvement of the space weather forecast quality. As the charged space environment affects the wide aspects of human civilization, the sustained monitoring of energized elementary particles is an important current task. Different methods and sensors are developed to provide measurements of particle fluxes at Low Earth Orbits (LEOs), geostationary orbits, and in the interplanetary space [1]. Silicon PIN, solid-state, surface barrier detectors, organic and inorganic scintillation detectors, large area photodiodes, multipixelated silicon photomultipliers are among them. The gamma- and X-ray detectors are often used to study non-steady variations in magnetospheric particle fluxes because of a bremsstrahlung generation by precipitating of subrelativistic electrons present in the upper layers of the atmosphere. We present in this work an example of simultaneous registration of particle streams by direct method and via bremsstrahlung of magnetospheric electrons aboard the CORONAS-Photon LEO satellite.

The CORONAS-Photon satellite was launched in January 2009 to the circular orbit with an inclination  $\sim 83^\circ$  and an altitude of about 550 km. Most of the payload was aimed at the study of a different manifestation of solar activity. The Satellite Telescope of Electrons and Protons STEP-F was intended to monitor the high energy charged particle fluxes. We present specific features in STEP-F constructing and

in SphinX solar photometer in X-ray range that had been installed aboard the CORONAS-Photon satellite too [2]. The SphinX instrument in its last ADC channels was capable to detect the low and intermediate energy particle fluxes both directly and through bremsstrahlung of the primary electrons. The axes of the directivity of the STEP-F and SphinX were mutually orthogonal.

Specific features in the construction of both instruments allowed revealing some interesting phenomena in radiation belts during one year of a minimum of 11 year's cycle of solar activity [3]. We present some results of data processing such as detection of the three-belt spatial structure of electron fluxes, lower limits of the energies for particle registration by the SphinX X-ray spectrophotometer, new ideas about contours of the South Atlantic Anomaly according to STEP-F particle detector measurements.

## Brief description of the STEP-F particle detector

Space experiment with the STEP-F instrument was aimed to study variations of high-energy electrons, protons, and  $\alpha$ -particles in the radiation belts, in the South Atlantic magnetic Anomaly and outside of them during magnetospheric storms, and to study the connection between trapped and precipitating particles of magnetospheric origin with the solar proton events and solar cosmic rays [4].

STEP-F consists of the detector unit STEP-FD, mounted outside the pressurized section of the spacecraft, and the digital signal processing unit STEP-FE, located inside the pressurized compartment. The STEP-FD



**Fig. 1.** A structural scheme of the detector head (a); the flight (b) and the breadboard (c) models of the STEP-F; the STEP-FD unit is among external detectors of the CORONAS-Photon satellite, as seen during vacuum tests (d)

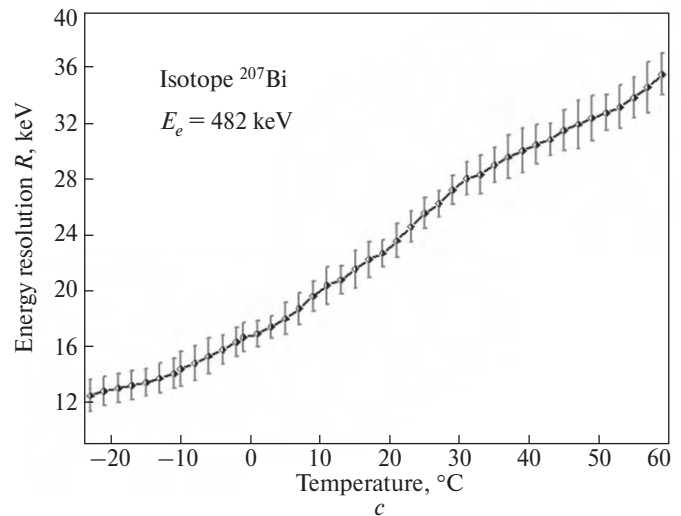
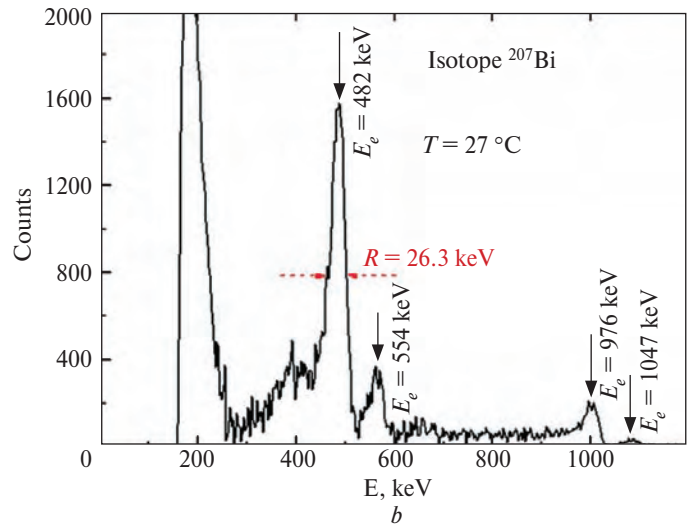
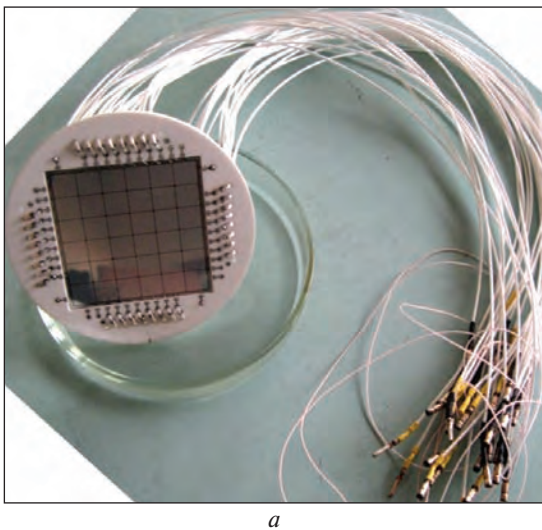


**Fig. 2.** The position-sensitive silicon matrix detector connected by soldering with thin coaxial cables outgoing from each matrix element (a); an example of the energy spectrum of conversion electron isotope source  $^{207}\text{Bi}$  obtained from one matrix element at a fixed temperature (b); the energy resolution  $R$  of matrix element for the energetic line  $E_e = 482\text{ keV}$  of  $^{207}\text{Bi}$ 's  $\beta$ -particles vs temperature (c)

unit consists of the detector head and 69 channels of analog signal processing. Each of the channels comprises charge-sensitive preamplifiers (CSA) and shaping amplifiers. The detector head of STEP-FD is designed as a telescopic system. Fig. 1 represents a structural scheme, different models of the STEP-F instrument, and placement of the STEP-FD unit among other external units of the payload of

CORONAS-Photon satellite during ground-based vacuum tests.

The detector head contains two identical silicon position-sensitive matrix detectors D1 and D2, each of them has an area of  $45 \times 45\text{ mm}^2$  and a thickness of 380 micrometers, and two scintillation detectors based on a CsI(Tl) single crystals viewed by the large area photodiodes in detector layer D3 and a vacuum

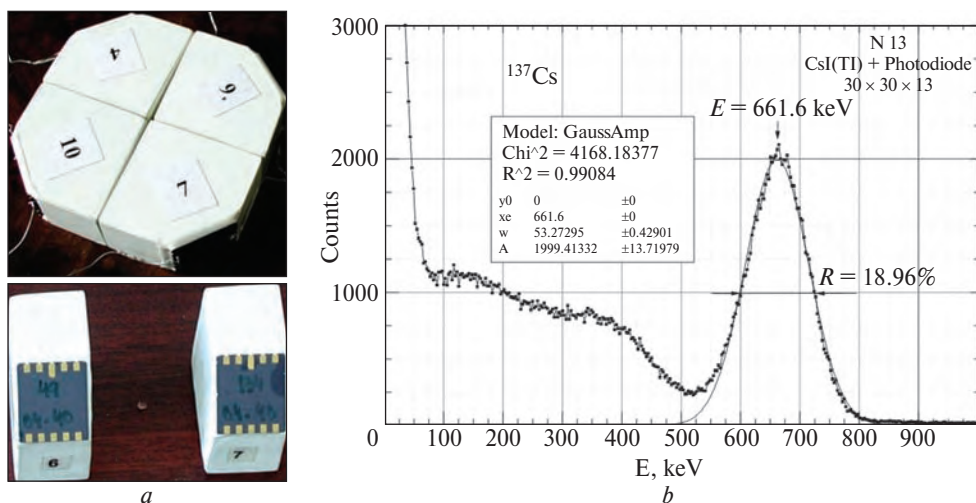


Fig. 3. Scintillation detectors coupled with the large-area silicon photodiodes (a); an example of  $^{137}\text{Cs}$  isotope gamma-quanta energy spectrum obtained from CsI(Tl) detector (b)

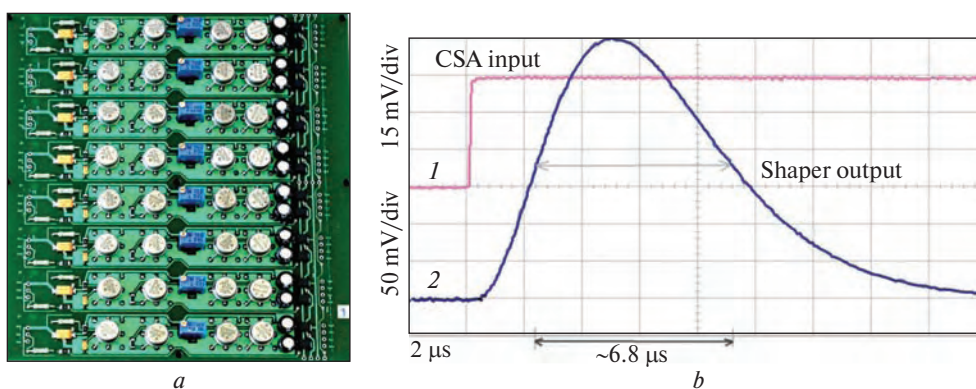


Fig. 4. A view of 8-channel' printed board of analog signal processing (a); the form of shaper' output quasi-gaussian signal as a response to step-like signal at the CSA test input (b)

photomultiplier in detector D4. The size of each of the 36 square elements of the silicon matrix detector is  $7.3 \times 7.3 \text{ mm}^2$ , which yields an average angular resolution of about  $8^\circ$  in the general field of view of the telescope for high-energy particles. Fig. 2 represents a common view of position-sensitive silicon matrix detector, an example of resulting measurements of one selected matrix element with the isotope  $^{207}\text{Bi}$  conversion  $\beta$ -particles, and the dependence of energy resolution for the energy  $E = 482 \text{ keV}$  on the temperature.

In Fig. 3 it is shown a common view of CsI(Tl) single crystal scintillation detectors of the D3 layer coupled with the silicon PIN large area photodiode, and example of  $^{137}\text{Cs}$  isotope gamma-quanta energy spectrum obtained from one of the D3 layer CsI(Tl) detectors.

Table 1 represents the energy ranges of registered electrons, protons and channels of mixed particle population.

Each element of the two silicon matrix detectors had their own analog signal processing channel. In

total, 64 channels mounted on eight printed boards served  $2 \times 32$  elements of matrices. In such a way we reached very high signal-to-noise, such that the total active area  $20 \text{ cm}^2$  of D1 and D2 layer comprised electronic noises equivalent of one element with the area of  $7.3 \times 7.3 \text{ mm}^2$ . The full width at half maximum (FWHM) of output from shapers' signals is of about 6.8 microseconds so that the upper limit of count rate for each element is at about  $f \approx 150 \text{ kHz}$ . In Fig. 4 the 8-channel' printed board of analog signal processing is shown and the form of the output signal as a response to the test step-like signal is plotted.

### The soft X-ray spectrophotometer SphinX

The structural scheme and a common view of the SphinX device are shown in Fig. 5. SphinX was equipped with four XR-100CR detectors provided by Amptek Inc., USA. These detectors were  $500 \mu\text{m}$  thick, pure silicon PIN diodes with entrance windows covered with  $12.7 \mu\text{m}$  thick beryllium foil. Each detector also had a temperature sensor, Peltier cooler, and FET transistor inside the package. Detectors

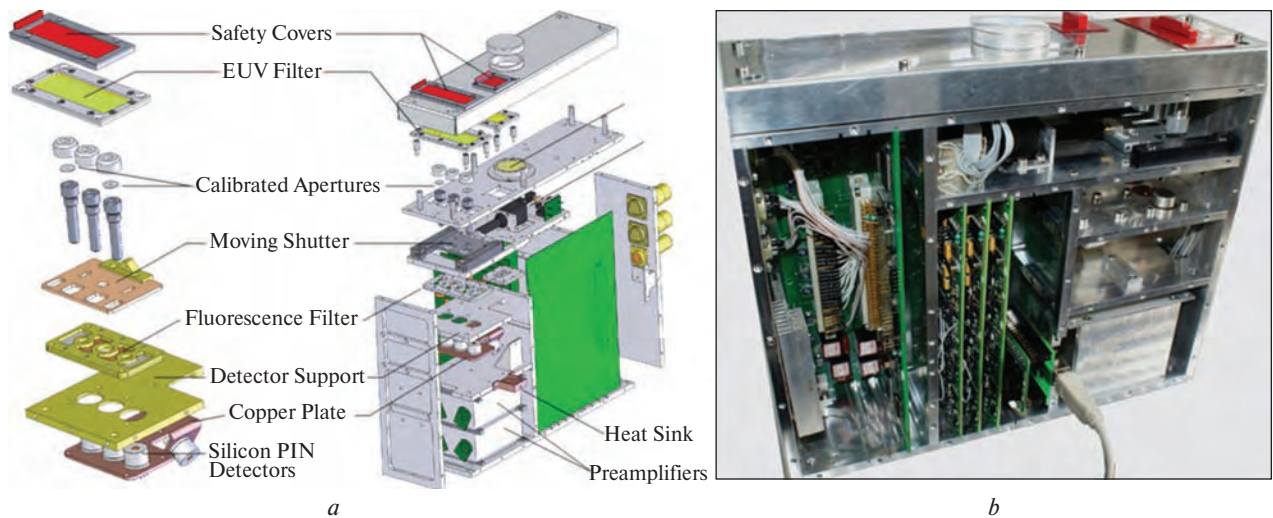


Fig. 5. Detailed structural scheme (a) and a common view of the soft solar X-ray spectrophotometer SphinX (b)

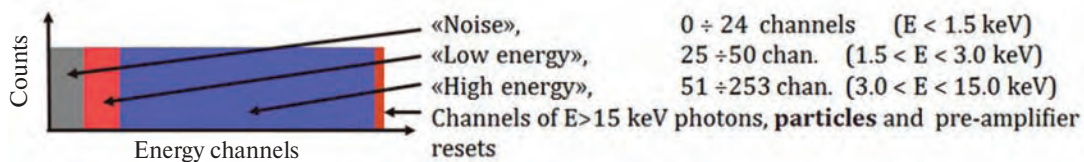


Fig. 6. Structure of information from SphinX in basic mode: 256-channel' energy spectra from D1 detector

were operated in flight at temperatures below  $-20^{\circ}\text{C}$ . Detector assembly came up with one detector (D1) of entrance aperture  $21.50\text{ mm}^2$  (the nominal factory entrance-window area), the second one (D2) with an aperture of  $0.495\text{ mm}^2$  for measuring moderate X-ray fluxes, and the third (D3) with an aperture of  $0.01008\text{ mm}^2$  for measurements of strong flux [5, 6].

Each measuring channel consisted of a detector, amplifier and shaper system whose output was read by an analog-to-digital converter and sent to an on-board computer. SphinX had spectral and event-counting modes of measurement. In the event-counting mode, every single pulse that appeared at the amplifier-shaper output was processed and information on the pulse amplitude and time of occurrence stored in memory. The pulse amplitude was converted to a

channel number in the spectrometer's 256 channel space. Thus, all multichannel analyzers had 256 energy channels covering the nominal energy range of  $0.0 - 15.0\text{ keV}$ .

Individual pulse-arrival times were determined with  $1\text{ }\mu\text{s}$  accuracy. The pulses had different origins. The pulse amplitude was proportional to the photon energy. Pulses were also produced when energetic particles hit the detector's sensitive volume. Another source of pulses was the measurement channel electronics itself. It had to be reset every couple of seconds. After resets, additional pulses were produced at the amplifier's output. Many particle- and reset-originating pulses had a large amplitude and thus are seen in the last SphinX energy channel (bin 256), which allows one to identify them.

Table 1

Energy ranges of registered electrons and protons

Particle sort	Energy range [MeV]	Remark
Electrons	0.35 – 0.95 1.2 – 2.3 > 2.3	Provided by D2 silicon matrix detector and two first energy channels of D3 CsI(Tl) scintillator
Protons	7.4 – 10.0; 15.6 – 55.2 in 9 channels; > 55.2	Provided by D2 silicon matrix detector and 10 energy channels of D3 CsI(Tl) scintillator
Electrons + protons	0.18 – 0.51 (electrons) + 3.5 – 3.7 (protons)	Channel of mixed particle registration
Electrons + protons	0.55 – 0.95 (electrons) + 3.7 – 7.4 (protons)	Channel of mixed particle registration

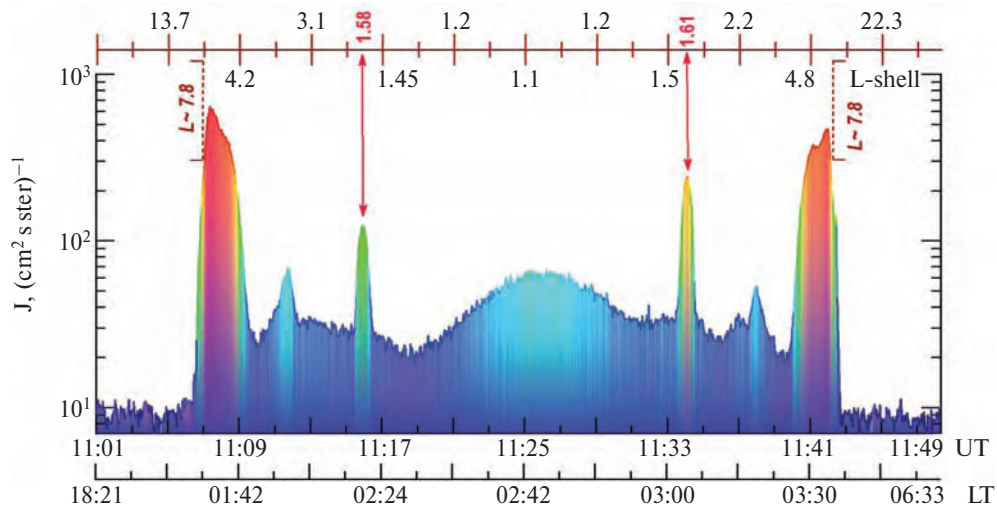


**Fig. 7.** Particle flux in the 1<sup>st</sup> channel of mixed particle registration (see Table 1) on May 6, 2009 on the ascending ascending part of the satellite orbit. UT is universal time; LT is local time

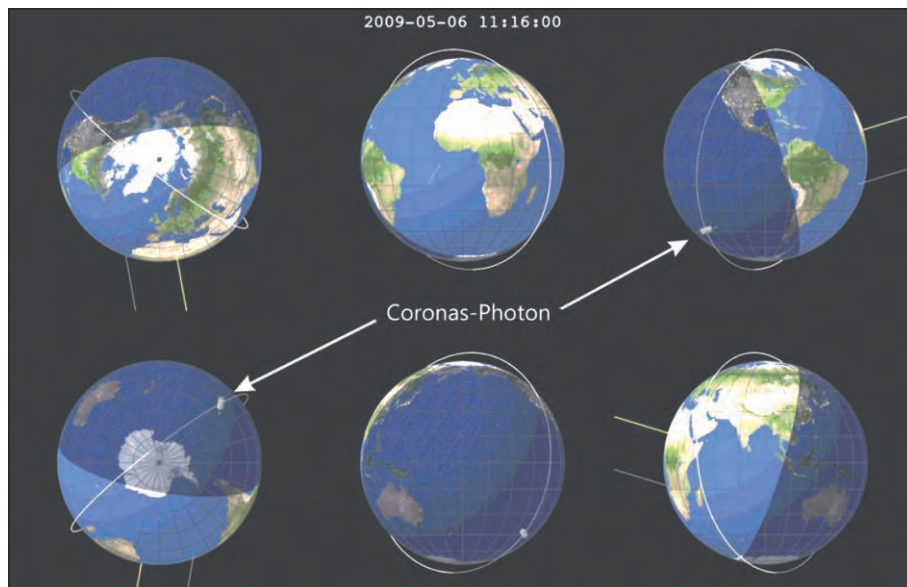


**Fig. 8.** Satellite position at the time of registration of the 3<sup>rd</sup> electron belt on May 6 in the Southern hemisphere

During the mission, SphinX recorded 256-channel and ancillary broadband, 4-channel spectra (so-called basic mode spectra). The first channel of the basic mode spectra contains mainly electronic noise. In the second and third channels solar X-ray flux was recorded in the energy ranges 1.5–3.0 keV and 3.0–14.9 keV for the D1 detector and 1.0–3.0 keV and 3.0–14.9 keV for the other detectors. The last channel of the basic mode contains the events caused by energetic particles and the instrument resets (Fig. 6).

### Some selected results of the data processing

Possessing high sensitivity to low particle fluxes the STEP-F instrument detected in 2009 a three belt's structure of electron fluxes in the channel of mixed particle registration (see Table 1). Fig. 7

represents data on electron fluxes in the energy range  $180 \text{ keV} \leq E_e \leq 510 \text{ keV}$  with 2-seconds' temporal resolution collected on the one of 15 ascending parts of the satellite orbit covering latitude range from  $-82.5^\circ$  South to  $+82.5^\circ$  North on May 6, 2009. Satellite crossed Van Allen outer and inner radiation belts in both hemispheres at the longitude range out from the South Atlantic magnetic Anomaly. Fig. 7 reveals presence of the third, additional belt being crossed by the satellite at  $L \approx 1.58$  in Southern hemisphere, and at  $L \approx 1.61$  in the Northern hemisphere. It is clearly seen that there is no vanishing quantity of low energy electrons within the magnetosphere at  $L \leq 7.8$  into whole latitude span, while the background fluxes of the particles outside the closed lines of geomagnetic field is less 3–6 times.

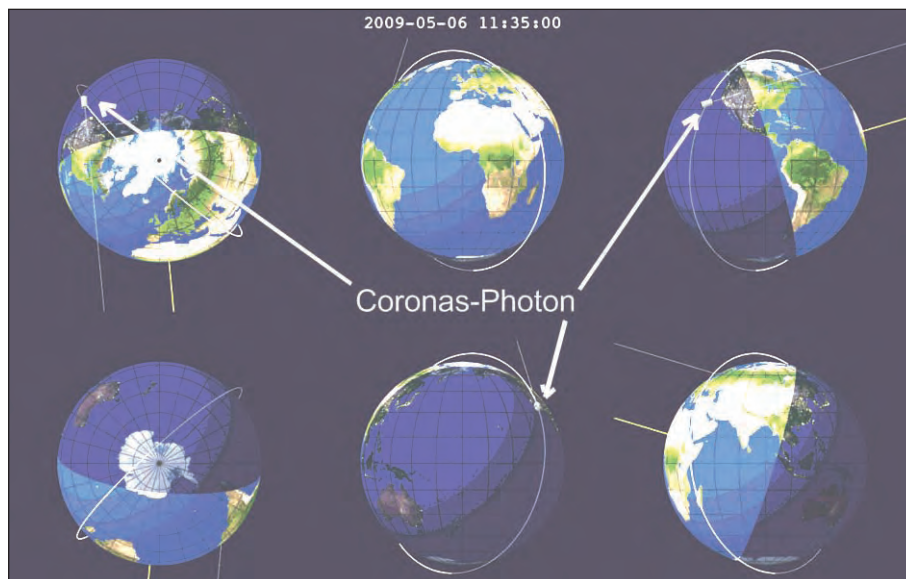


**Fig. 9.** Satellite position at the time of registration of the 3<sup>rd</sup> electron belt on May 6 in the Northern hemisphere

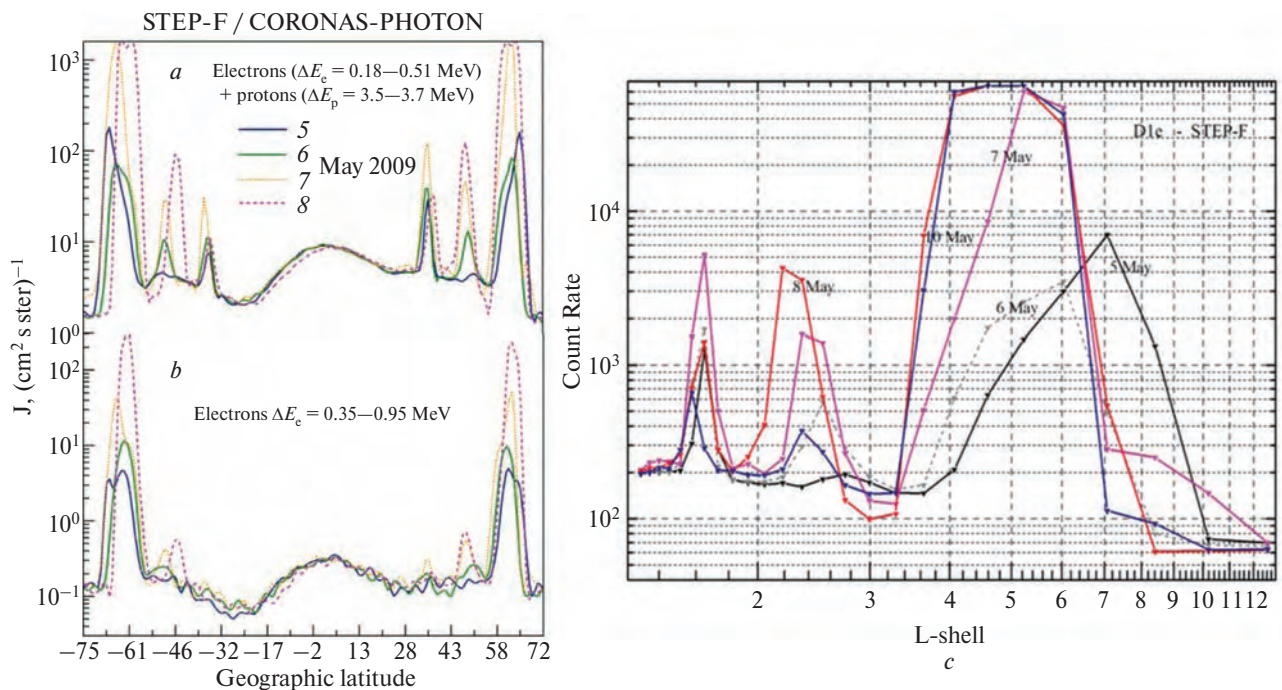


**Fig. 10.** Particle fluxes in the channel of mixed particle registration (a) and in the electron channel of energies  $\Delta E = 0.35\text{--}0.95$  MeV (b) over the period of 5–10 May 2009. Different colors / lines represent individual days as indicated. (c) is distribution of particle fluxes by McIlwain  $L$ -shells

Fig. 8 and Fig. 9 demonstrate satellite position at the times of registration the 3<sup>rd</sup>, additional inner electron radiation belt at  $L \approx 1.6$  in both hemispheres during the low solar and geomagnetic activity of May 2009. Each frame consists of 6 views. From the left to right a view from the North Pole and at Equatorial plane at 0 and 180 degrees of the longitudes is shown on the top row. The view from the South Pole and at Equatorial plane at 90 and 270 degrees of the longitudes is shown on the lower series from the left to right too.

As it can be seen from both Figures the additional inner electron radiation belt was observed at nighttime of the LT, far from the South Atlantic Anomaly zone.

Fig. 10 represents data with 30-seconds' temporal resolution collected on every 9<sup>th</sup> ascending parts of satellite orbit over the period from May 5 to May 10, 2009. Also, Fig. 10 reveals presence and stability of the registration of the third, additional inner belt being crossed by the satellite at  $-35\div-32$  degrees South, and at  $\sim 36\div 42$  degrees North.

The persistent presence of the third belt on lower  $L$ -shell and the temporal variation of electron population in both belts are observed depending on the overall level of geomagnetic activity.

The two inner radiation belts on  $L \approx 2.28$ , and  $L \approx 1.61$  were detected in the energy band  $\Delta E_e = 0.18 \div 0.51$  MeV, the other particle channels did not confirm the fact of presence of the new belt. It can be concluded that the narrow belt at  $L \approx 1.6$  is populated by the particles with energies not higher than 0.5 MeV.

Both inner radiation belts are seen on geographical longitudes that do not coincide with the South Atlantic Anomaly longitudes.

We carried out the comparison of the data extracted from the highest ADC channel of the SphinX spectrophotometer with the STEP-F recordings. As a result, Det1 and Det2 detectors of SphinX are sensitive to electrons and the secondary  $\gamma$ -quanta, generated by the magnetospheric high energy electrons. The latter allowed us to introduce the concept of effective lower energy thresholds for electron registration ( $E_{thr1}$  and  $E_{thr2}$ ) by Det1 and Det2 detectors, respectively.

The analysis of averaged over 14 days of May 2009  $L$ -shell values with maximum particle count rates vs. electron energy allowed us to determine values of effective lower threshold energies  $E_{thr1}$  and  $E_{thr2}$ . We determined also the lower threshold energy of the D4e channel, where D4 is the bottom-most scintillation detector of the STEP-F instrument' detector head. In Fig. 11 it is shown a dependence of  $L$ -shells with the largest particle fluxes, as a function of the electron energy for the South Atlantic Anomaly region. As a basic point the energies of D2e (electrons with energies  $E_e = 0.35 \div 0.95$  MeV) and D1p (electrons with energies  $E_e = 0.55 \div 0.95$  MeV + + protons with energies  $E_p = 3.7 \div 7.4$  MeV) energy channels of STEP-F were chosen.

Fig. 11 demonstrates that the values of  $E_{thr1}$  and  $E_{thr2}$  are closely near, assumed values  $\sim 500$  keV and  $\sim 475$  keV for Det1 and Det2 of SphinX, respectively. Large dispersion of these values is determined by a poor

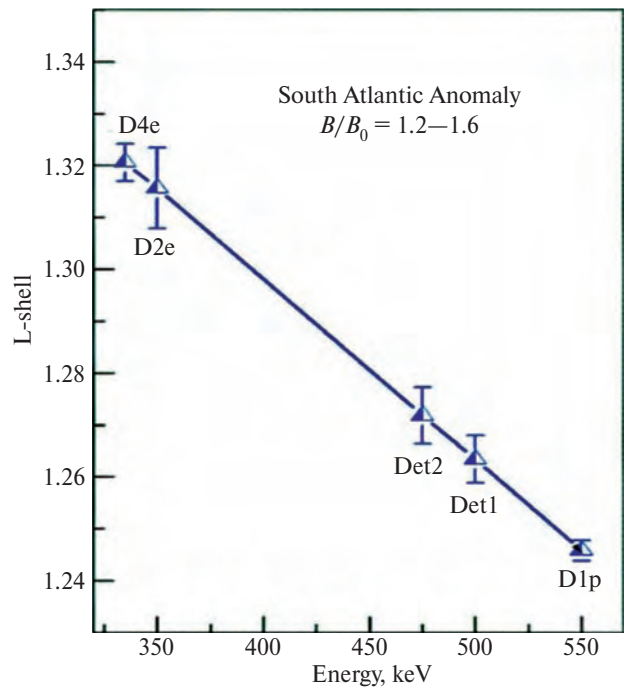


Fig. 11. Dependence of averaged  $L$ -shell values corresponding to maximum electron flux densities on the particle energy

statistic (14 days analyzed), from one side, and by the diurnal displacement of the satellite position on the longitude at fixed latitude relative to the initial day.

The bottom threshold energy of the D4e channel of STEP-F device is  $E_{D4e} \approx 335$  keV as can be seen in Fig. 11.  $E_{D4e}$  values varied from day to day in the energy range from 230 to 350 keV during May 1–14, 2009, probably due to variation of electron energy spectrum slope.

### Contours of the South Atlantic Anomaly as seen by STEP-F

The CORONAS-Photon orbit crosses all longitudes between  $\pm 82^\circ 15'$  during the diurnal period. This allowed us to construct daily maps of the particle content at the height of  $\sim 550$  km in terms of high energy charged particle fluxes. Such an approach for

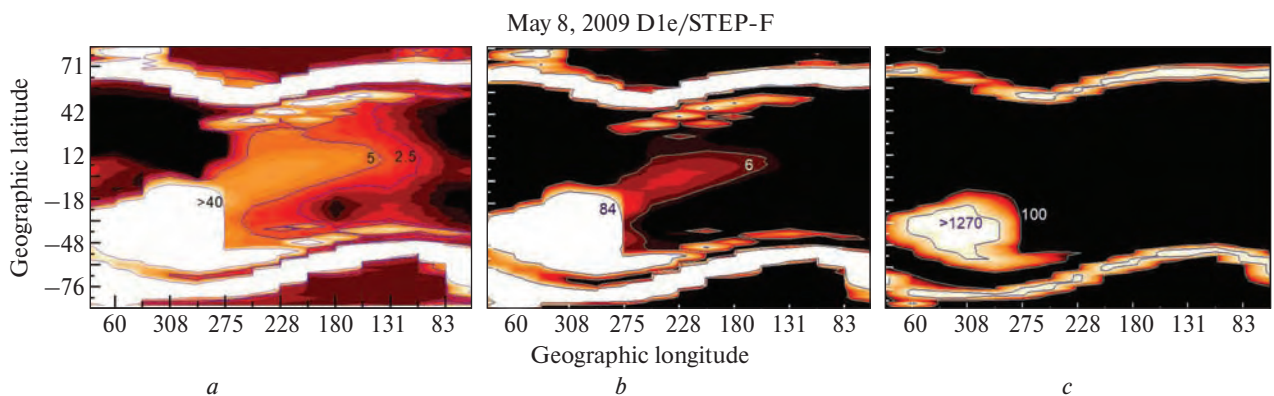


Fig. 12. A view of the SAA and radiation belts as seen by STEP-F in various intensity ranges. Explanations are given in the text

the electrons in the energy range  $\Delta E_e = 0.18 \div 0.51$  MeV gave us the possibility to see the contours of the South Atlantic Anomaly having in mind high sensitivity of STEP-F to extremely low particle fluxes and the binding of the particle trajectories to the geomagnetic field lines.

Results of the 1<sup>st</sup> channel of mixed particle registration (see Table 1) data processing applied for May 8, 2009, are shown in Figure 12. The three maps in a shade of red are presented for particle intensity limits from 1 to 40 (Fig. 12, *a*), from 5 to 100 (Fig. 12, *b*) and from 100 to 1500 (Fig. 12, *c*) electrons / cm<sup>2</sup>s sr.

The higher the strength of the geomagnetic field in the region of the SAA, the more precipitating electrons are recorded by the STEP-F (Fig. 12, *c*). But negligible fluxes of precipitating particles are seen in the near equator zones up to projections of inner radiation belts onto altitude of the satellite trajectory in the northern hemisphere in a wide range of geographic longitudes from  $\sim 120$  to  $\sim 275$  degrees (Fig. 12, *a*). Whereas the azimuthal drift of electrons according to the 3<sup>rd</sup> adiabatic invariant it is envisaged that the SAA dimensions are much larger in comparison with the current classical concept.

### Conclusions

1. Specific uncommon technical solutions adopted in the construction of the Satellite Telescope of Electrons and Protons STEP-F and the solar soft X-ray spectrophotometer SphinX allowed finding out some new patterns in the behavior of the high energy charged particles of the magnetospheric origin. Particularly, the utilization of silicon matrix-type configuration in the first two detecting layers of the STEP-F detector head allowed reaching a very high signal to noise ratio. This led to the detection of very weak particle fluxes outside of the regions of Van Allen outer and inner radiation belts and SAA including low latitudes and near-equatorial zone. Recording of the scientific information in the SphinX' spectral mode allowed finding extremely useful data in the last channel of the energy spectra on the variations of low and intermediate energies particles in the Earth's magnetosphere. Cross-analysis of data derived from both instruments led to estimating of

the effective lower energy thresholds for primary particles seen by the SphinX sensors in the last ADC channel.

2. Specific features in the design of both spaceborne based instruments enabled us to reveal the existence of new (third) steady electron radiation belts located below the Van Allen electron inner belt, on  $L \approx 1.6$  for particle energies  $E \leq 500$  keV, with significantly varying particle fluxes in response to a weak substorm in the magnetosphere. New ideas about dimensions of the South Atlantic Anomaly through the STEP-F particle detector measurements have been developed.

### REFERENCES

1. Dudnik O. Radiation environment at Low Earth Orbits. *Consultations on modelling and analysis of orbital background in X-ray detectors*. September 19–20, 2019. Wrocław, Poland. Programme. [http://www.cbk.pan.wroc.pl/conferences/meeting\\_2019/meeting\\_2019.html](http://www.cbk.pan.wroc.pl/conferences/meeting_2019/meeting_2019.html).
2. Dudnik O.V., Sylwester J., Kowaliński M., Barylak J. Utilization of design features of the particle telescope STEP-F and solar x-ray spectrophotometer SphinX for exploration of the Earth's radiation belt properties. *Proceedings SPIE*. 2019. Vol. 11176 "Photonics Applications in Astronomy, Communications, Industry, and High-Energy Physics Experiments". P. 111763L-1–111763L-10. <https://doi.org/10.1117/12.2537296>.
3. Dudnik O.V., Sylwester J., Podgórski P. Combined study of radiation belts by the satellite particle telescope STEP-F and solar soft X-ray photometer SphinX during recent deep minimum of solar activity. *Proceedings of 23<sup>rd</sup> National Slovak Solar Physics Meeting*. Liptovský Mikuláš, Slovakia, 30 May – 3 June, 2016. ISBN 978-80-85221-92-3 (on DVDs). Publisher: Slovak central observatory, Hurbanovo. P. 1–6.
4. Dudnik O.V., Persikov V.K., Zalyubovskiy I.I., Timakova T.G., Kurbatov E.V., Kotov Yu.D., Yurov V.N. High-sensitivity STEP-F spectrometer—telescope for high-energy particles of the CORONAS-PHOTON satellite experiment. *Solar System Research*. 2011. Vol. 45, Iss. 3, P. 212–220. <https://doi.org/10.1134/S0038094611020043>.
5. Gburek S., Sylwester J., Kowalinski M., Bakala J., Kordylewski Z., Podgorski P., Plocieniak P., et al. SphinX soft X-ray spectrophotometer: science objectives, design and performance. 2011. *Solar System Research*. Vol. 45, Iss. 3, P. 189–199. <https://doi.org/10.1134/S003809461102006>.
6. Gburek S., Sylwester J., Kowalinski M., Bakala J., Kordylewski Z., Podgorski P., Plocieniak S., et al. SphinX: The Solar Photometer in X-Rays. *Solar Physics*. 2013. Vol. 283, Iss. 2. P. 631–649. <https://doi.org/10.1007/s11207-012-0201-8>.